Exp Tech (2016) 40:1511–1525
DOI 10.1007/s40799-016-0107-8

Different Measurement Techniques for Wider Small Radial Turbine Performance Maps

G. Salameh[1] · **P. Chesse**[1] · **D. Chalet**[1]

Received: 11 January 2016 / Accepted: 11 April 2016 / Published online: 20 July 2016
© The Society for Experimental Mechanics, Inc. 2016

Abstract Engine downsizing usually requires the use of a turbocharger. This component's related data are reduced. This is caused by the small range of stable functioning of its centrifugal compressor at high boost pressures. That is why the measurement of the data of both the compressor and the turbine is limited. Numerical simulations are used by automotive manufacturers for internal combustion engines simulations, so it is necessary to have an accurate and reliable extrapolation model of the turbine performance maps. Once an extrapolation model is established, the new performance map can be used for internal combustion engines calibration. This study presents different experimental techniques to measure the widest performance map of a small radial turbine. This turbine is a part of a turbocharger of a small diesel engine. Experiments were held on a traditional turbocharger test rig at first. The turbine inlet temperature was changed to extend the mass flow rate measurement range. Then there was the compressor force-feeding where air was blown through the compressor inlet and exit. This technique allowed the extension of the map by increasing and decreasing the power consumed by the compressor rotor and moving its surge and choking limits. After that, the compressor was replaced by another one with a reversed rotational direction. Blowing air to the new compressor exit enabled us to use it as a turbine and hereby extend the data map. We measured very low mass flow rates using a hot wire anemometer. This sensor also allowed us to measure negative mass flow rates to reach the expansion ratio of one zone. These techniques gave an almost complete mass flow rate performance map with an expansion ratio going from 1 to 6 for some rotational speeds. As for the efficiency, data were measured in adiabatic conditions. This allowed the calculation of the turbine total-to-static isentropic efficiency and the turbocharger mechanical efficiency separately. These data enabled us to calculate the turbine efficiency according to the manufacturer's method.

Keywords Turbocharging · Radial turbine · Experiments · Performance map · Mass flow rate · Efficiency · Compressor

Definitions/Abbreviations

D_m	mass flow rate, kg/s
$D_{m\text{-}corr}$	corrected mass flow rate, kg/s
N	rotational speed, rpm
N_{corr}	Corrected rotational speed, rpm
p	static pressure, bar
p*	total pressure, bar
P_{ref}	Reference pressure
T	static temperature, K
T*	total temperature, K
h*	Total enthalpy, J/kg
T_{ref}	Reference temperature
h	Enthalpy kJ/kg
η	efficiency
$c_{p\text{-}air}$	air specific heat at constant pressure, kJ/kg.K
A	section, m^2
P	Power, W
Q	Heat transfer

Subscripts

turb	turbine
comp	compressor
in	inlet

✉ G. Salameh
georges.salameh@ec-nantes.fr

[1] Ecole Centrale de Nantes, LHEEA Lab. (ECN/CNRS), BP92101, Nantes Cedex 3, France

out	exit
meca	mechanical
t-s	total-to-static
isentr	isentropic
avr	average
corr	corrected
red	reduced

Introduction

Today turbocharging technology is used in all diesel engines. This technology is today also spreading to controlled ignition engines. Downsizing and turbocharging are efficient technologies to reduce engines consumption and emissions. Even though the use of turbochargers is widespread, their performance over the whole operating area is not well known and their use in internal combustion engines is consequently affected.

Internal combustion engines calibration is then the main reason to have a complete set of turbine and compressor performance data maps covering all the operating area. Since numerical simulations are the main tool used by automotive manufacturers for internal combustion engines simulations (new engines architectures, ECU, HIL, engine calibration as mentioned above), it is essential to have an accurate extrapolation model generating a complete turbine performance map.

Different studies focused on turbine performance maps measurements. Performance maps given by the turbocharger manufacturer are usually measured according to the procedure of *Turbocharger Gas Stand Test Code, J1826 SAE* [1]. This is a hot-gas-test-bench. There are two configurations of this test bench: open loop and closed loop. Usually the open loop configuration is preferred. This is almost the same procedure used in this paper to measure the turbine and compressor performance maps in the case of turbine inlet temperature of 550 °C.

Many turbocharger test benches were developed including the one used by Venson and Barros [2] where the turbine is first powered by a radial compressor and the turbocharger compressor exhausts to the atmosphere. This method makes possible to measure data for low speeds and low expansion ratios and pressure ratios. In the second configuration, the turbine is powered by both the external compressor and the turbocharger compressor: in this case, it is possible to explore intermediate pressure ratios and rotational speeds. Finally, the turbocharger is operated independently in a way that the turbine produces enough power to let the compressor alone supply the combustion chamber with air. It is possible with this configuration to measure real and extreme operating points.

In the study of Otobe et al. [3], an experimental study allows to measure the turbocharger performance data at low rotational speeds. A turbocharger with water cooling system is used and with every water and oil temperature new data were measured. Friction losses were also evaluated. Deligant et al. [4] also deals with mechanical friction losses. In this study, the turbocharger friction losses are quantified and hereby the power produced by the turbine and consumed by the compressor. Deligant et al. [5], Lamquin and Gjika [6], and Podevin et al. [7, 8], also deal with turbocharger friction losses evaluation.

In their work, Scharf et al. [9] present a complete study about the turbocharger performance map extension. The first technique consists in using the compressor in a closed loop configuration. Its absorbed power increases and hereby measurement of higher expansion ratios on the turbine side is performed. The compressor is also used in another configuration: the compressor wheel is replaced by a bladeless disk. Hence, it is possible to get data for low expansion ratios. To extend the turbine map range to low turbocharger speeds, a dynamometer test bench was used: the compressor is replaced by a speed controlled electrical brake and the net torque is measured. Friction measurements can also be used to evaluate the turbocharger friction losses and hereby separate the turbine efficiencies: turbine isentropic efficiency and mechanical efficiency.

Other studies on the turbine performance maps measurements such as Dale [10] who developed experimental studies on unsteady flow in radial turbines. A hydraulic dynamometer was also used by Winterbone et al. [11] and Nikpour [12] for torque measurement. A radial compressor was used by Arcoumanis et al. [13] to absorb the increasing power of larger turbines. For torque measurement, Szymko [14] developed an eddy current dynamometer designed for low known inertia of the rotating assembly that is able to absorb the turbine power. Hence the measurement accuracy of instantaneous torque [15] is increased. Galindo et al. [16] used the compressor as a breaking device: a narrow range of data is available due to the surge limit and choking limits of the compressor. This is the main disadvantage of the performance maps given by the manufacturer. It is also a common thing to characterize turbine maps using the whole turbocharger assembly as for the OEMs [1, 17].

A common problem in the turbine performance maps given by the manufacturer is the narrow measurement area. This is caused by the compressor: the first limit is the surge line that appears on the left side of the compressor performance map (hence at low mass flows). The second limit is the choke limit which appears on the right side of the compressor map (high mass flows). Despite the fact that the problem is caused by the compressor side, the turbocharger performance measurements should be done on the entire turbocharger as much as possible to keep the coupling between the compressor and the turbine, and also to maintain the equilibrium of the system.

To extend these narrow measurement areas on the manufacturers turbine performance maps, extrapolation methods are applied: these methods could be mathematical with a simple curve fitting and a polynomial or exponential expression. They can be more complex like zero or one dimensional

models or even three dimensional studies (ex: CFD tools). Watson and Janota [18] presented a simple model for a radial turbine: the turbine is represented as a nozzle at the engine exhaust. Payri et al. [19] also presented the turbine as a nozzle, such as Winterbone [20] who used the concept of the effective area. The model of Hibernick et al. [21] for the double entry turbines uses pipe junctions. Another model of Payri et al. [22, 23] representing the turbine as two nozzles in series separated by an intermediate volume is also presented. A model of mixed flow turbines under pulsating flow conditions is also presented by Chen et al. [24]. Radial turbine models are also studied in the two cases: fixed blades with Macek et al. [25] and moving blades with Nasser and Playfoot [26].

Other studies such as the thesis of M. Frelin [27] focus on varying the turbine inlet temperature and therefore the air density. This latter change allows to measure a wider range on the turbine performance map as we will see further in this paper.

The turbocharger performance maps given by the supplier are generally represented with corrected values or reduced values. For the turbine, there are two performance maps: one for the mass flow and the other one for the efficiency. The turbine expansion ratio is the ratio of the turbine total inlet pressure to the turbine total exit pressure. Regarding the mass flow rate, it is either corrected as we can see in (equation (1)), or reduced as we can see in (equation (3)). Same goes for the rotational speed: it is either corrected (equation (2)) or reduced (equation (4)). In this study, we will use the corrected values.

$$D_{m-corr} = D_m \times \frac{\sqrt{\frac{T^*_{in,turb}}{T_{ref}}}}{\frac{P^*_{in,turb}}{P_{ref}}} \tag{1}$$

$$N_{corr} = N \times \sqrt{\frac{T_{ref}}{T^*_{in,turb}}} \tag{2}$$

$$D_{m-red} = D_m \times \frac{\sqrt{T^*_{in,turb}}}{P^*_{in,turb}} \tag{3}$$

$$N_{red} = \frac{N}{\sqrt{T^*_{in,turb}}} \tag{4}$$

The compressor performance is shown in one map where we have the pressure ratio, the compressor corrected mass flow rate and the compressor isentropic efficiency for every corrected rotational speed. On this map, it is possible to localize the surge line and the choking limit. They are the two limitations preventing the measures to go further on the compressor performance. The compressor pressure ratio is the ratio of the compressor total exit pressure to the compressor total inlet pressure. An example of a compressor performance map is presented in Fig. 3.

This paper presents an experimental approach to get an almost complete turbine mass flow rate performance map and an extended map of the turbine efficiency. The first technique used will be the turbine inlet temperature variation. Then there will be the compressor force-feeding where air will be blown to the compressor inlet and exit respectively. Afterwards, the compressor will be replaced by another one with a different configuration to extend the measurement area. The small flows will be measured with a hot wire anemometer. There will also be a measurement of negative flow in the turbine for points close to an expansion ratio of one. Once all these curves are connected, we get almost a complete turbine mass flow rate performance map for an expansion ratio going from 1 to 5.5 for some rotational speeds. As for the turbine efficiency, there will be a measurement based calculation of the turbine isentropic efficiency, a turbocharger mechanical efficiency and a conventional turbine efficiency (isentropic efficiency * mechanical efficiency).

Turbine Mass Flow Rate Measurement Techniques

Entire Turbocharger Study

The turbocharger test bench used in this study is located in the LHEEA lab. (Laboratoire Hydrodynamique, Energétique et Environnement Atmosphérique) at Ecole Centrale de Nantes in France.

In this section, the turbocharger is tested as a whole: the turbine and the compressor are not modified but the measurement techniques change. There are mainly three techniques in this part: the turbine inlet temperature variation, the compressor inlet forced-feeding, and the compressor exit forced-feeding.

Turbocharger presentation

The turbocharger studied here is a small fixed geometry turbocharger for a small diesel engine. Its performance maps given by the manufacturer are very narrow.

The turbine is a fixed geometry radial turbine with 12 blades on the rotor. The exhaust air coming from the engine goes into the turbine volute and the distributor which is an extension of the volute, and then into the rotor. Air is then exhausted from the turbine in an axial direction after the expansion. The turbine inlet and exit cross sections are 726 mm^2 and 1295 mm^2 respectively.

The compressor is centrifugal. The fluid enters the compressor in an axial direction and exits in a radial direction. The inlet and the exit sections are respectively 962 mm^2 and 789 mm^2. The fluid goes through the impeller and then through the diffuser to the volute.

As shown in Fig. 1, the turbine is driven by compressed air going through an electric heater [192KW], which regulates the turbine inlet temperature. The turbine mass flow rate and its expansion ratio are controlled with an electric vane at the turbine inlet. The source of the test rig's compressed air is a screw compressor with maximum pressure of 7.5 bar and maximum flow rate of 0.24 m^3/s. This compressed air goes through a 405 CF carbon filter and a drier before going into the heater. The exhaust air is rejected outside using an extractor fan. A pressure regulator is also used at the turbine inlet to avoid pressure overshoots.

As for the compressor, inlet air is filtered, and its flow rate is measured with a mass flow meter. The air mass flow and the pressure ratio across the compressor are controlled using an electric vane at the compressor exit. The compressor exhaust air is also rejected to the outside with the same extractor fan used on the turbine side.

The turbine and compressor mass flow meters use both vortex technologies (Krohne optiswirl 4070C). Their measurement error goes up to ±2.5 % of the measured value depending on the flow's Reynolds number. Their measurement range goes from 50 to 550 kg/s. The difference between the two flowmeters is that the one used on the compressor side can measure mass flow rates at low pressure which is the case at the compressor inlet.

On this turbocharger test rig, the first measurements aimed at the construction of a performance data map in conditions close to those of the manufacturer. The turbine inlet temperature is 550 °C, the oil inlet temperature is 90 °C and the oil inlet pressure is 3 bars. Inlet compressor pressure and temperature are at ambient conditions. The results are shown in Fig. 2: we can note the narrowness of each corrected rotational speed curve.

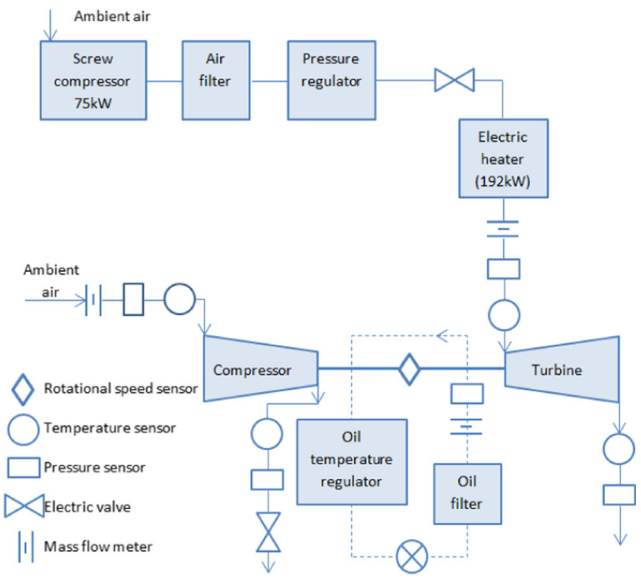

Fig. 1 Turbocharger test rig

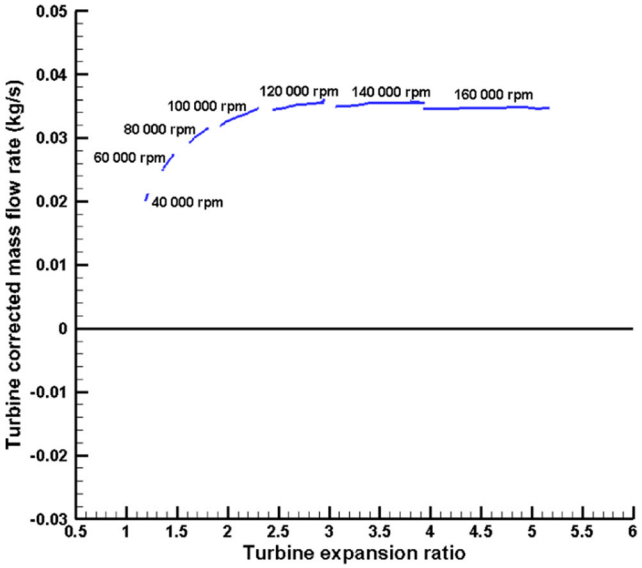

Fig. 2 Turbine corrected mass flow rate vs. turbine expansion ratio for different corrected rotational speeds at turbine inlet temperature 550 °C

It is important also to mention that the manufacturer's data are even narrower than these since the manufacturer's data map does not contain the curves at 40 000, 60 000 and 160 000 rpm (corrected speed). Figure 3 shows the compressor data map measured with the turbine in these conditions. This measurement is the starting point to get an almost complete mass flow rate data map. Many techniques will be presented in this paper starting with the turbine inlet temperature variation (Table 1).

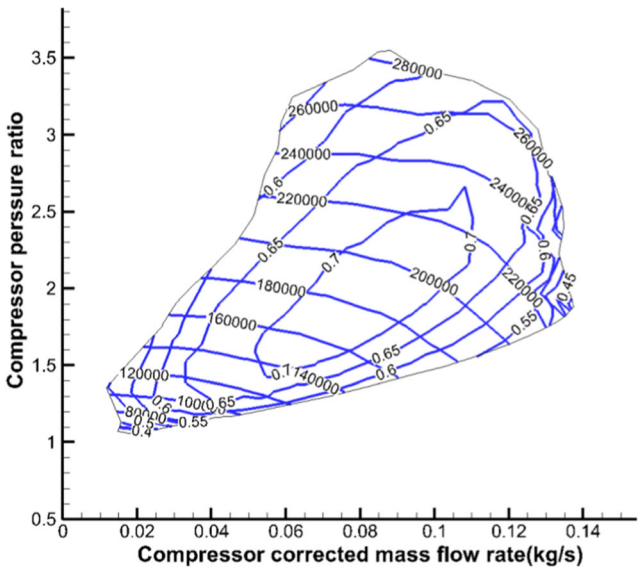

Fig. 3 Compressor data map: compressor pressure ratio vs. corrected mass flow rate for different corrected rotational speeds and isentropic efficiencies

Table 1 Color index for different turbocharger test bench techniques

$T_{in,turb}$=550°C (Turbine inlet temperature variation)	**Blue _**
$T_{in,turb}$=300°C (Turbine inlet temperature variation)	**Green _**
Adiabatic conditions (Turbine inlet temperature variation)	**Purple _**
Compressor inlet forced-feeding; $T_{in,turb}$=300°C	**Orange _**
Compressor inlet forced-feeding; adiabatic	**Light**
Compressor exit forced-feeding; $T_{in,turb}$=300°C	**Black _**
Compressor exit forced-feeding; $T_{in,turb}$=100°C	**Brown _**
Compressor replacement (mass flow meter)	**Cyan _**
Compressor replacement (Hot wire anemometer: positive mass flow rate)	**Mauve _**
Compressor replacement (Hot wire anemometer: negative mass flow rate)	**Red _**

Turbine inlet temperature variation

Changing the turbine inlet temperature is a technique to extend the mass flow rate measurement due to the change of the air density in the turbine. When the air density is changed, the measuring area on the performance map is also changed. Once the mass flow rate is measured at the different temperatures, it is possible to link the curves and get an extended curve as shown in Fig. 4.

The second turbine inlet temperature (after the 550 °C) is the "adiabatic" temperature: adiabatic temperature means a low temperature to minimize the heat exchanges in the turbocharger and get as close as possible from the adiabatic conditions in both the compressor and the turbine. In the turbocharger, there are many heat transfers but the ones mainly considered in this part are: the heat exchange between the air in the turbine and the air in the compressor, between the oil and the air inside the compressor, between the oil and the air inside the turbine, and finally between the whole turbocharger and its surrounding environment. Many studies were done on the subject of the adiabatic conditions, such as the works of Cormerais et al. [28, 29]. The choice of the experimental hypothesis for an adiabatic process was to equalize the turbine average temperature with the compressor average temperature and the oil inlet temperature (equation (7)). The turbine average temperature is the arithmetic average of the turbine inlet and exit temperature (equation (6)). The same calculation is done for the compressor average temperature (equation (5)).

$$T_{avr-comp} = \frac{T_{in,comp} + T_{out,comp}}{2} \tag{5}$$

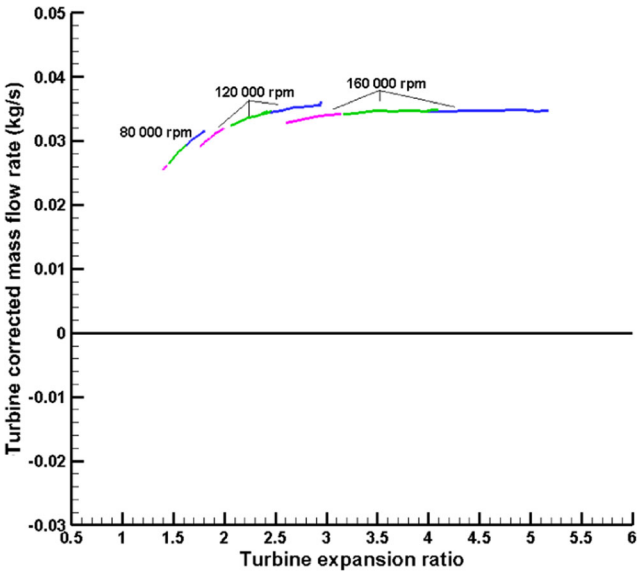

Fig. 4 Turbine corrected mass flow rate vs. turbine expansion ratio for different corrected rotational speeds at turbine inlet temperature 550 °C (*blue*), 300 °C (*green*) and adiabatic (*purple*)

$$T_{avr-turb} = \frac{T_{in,turb} + T_{out,turb}}{2} \quad (6)$$

$$T_{avr-comp} = T_{avr-turb} = T_{in-oil} \quad (7)$$

The third turbine inlet temperature is 300 °C: this temperature is considered as an intermediate value between the high temperature conditions (550 °C) and the adiabatic conditions. The data measured at 300 °C gives a series of points in an intermediate position between the data measured at 550 °C and the "adiabatic" data as shown in Fig. 4. The curves of 550 °C and "adiabatic" measurements are now linked by the data at 300 °C.

Figure 4 represents the extension of the corrected mass flow rate curves for three corrected rotational speeds using the turbine inlet temperature variation. This is the first technique presented in this paper for the turbine performance map extension. This extension was obtained for the compressor performance map as well as the turbine performance map.

Compressor forced-feeding

The main reason of the turbine narrow data performance map is the compressor behavior. The compressor measurements are limited on both sides: the surge limit and the choke limit. The compressor forced-feeding is a technique to increase its power consumption. The power consumed by the compressor is produced by the turbine so with this technique it is possible to extend the turbine and compressor performance maps. The forced-feeding can be applied by blowing air into the compressor inlet or exit. Each technique has a different impact.

Compressor Inlet Forced-Feeding The turbine and compressor performance maps are limited by the power consumed by the compressor as mentioned before, and a main reason for this limitation is the air density at the compressor inlet. When the compressor runs at certain speeds and does not have enough air going through it, its power consumption is blocked. By blowing air into the compressor inlet, it was possible to increase the air density in the compressor and hereby increase the compressor power consumption and the turbine power production. The compressed air comes from the screw compressor supplying the turbine but this air is not heated. This technique gave a turbine and compressor map extension to the right side. The result is a higher mass flow rate for higher pressure ratio in the compressor and higher expansion ratio in the turbine. These measurements were done at a turbine inlet temperature of 300 °C and in adiabatic conditions (as described above).

Figure 5 shows the results for the compressor inlet forced-feeding at a turbine inlet temperature of 300 °C. The curves are extended to the right of the previously measured data at 300 °C (turbine inlet temperature) as predicted for this technique. The power consumed by the compressor is greater and the choke limit is shifted.

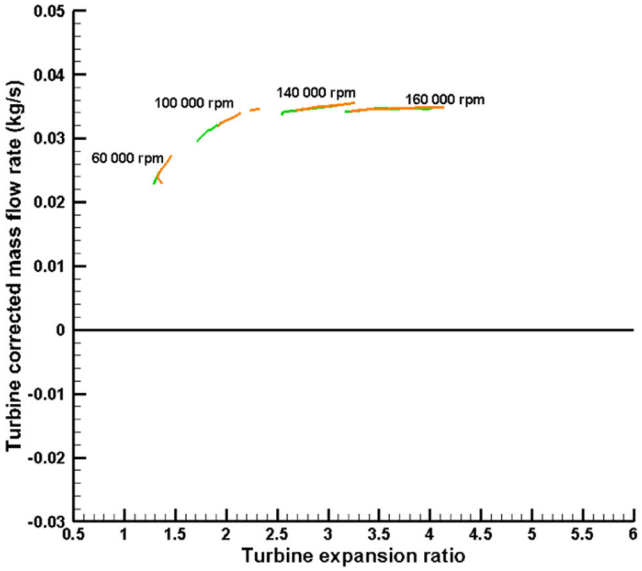

Fig. 5 Turbine corrected mass flow rate vs. turbine expansion ratio for turbine inlet temperature 300 °C (green), and compressor inlet forced-feeding at turbine inlet temperature 300 °C (*orange*)

Then measurements in adiabatic conditions were done with the technique of the compressor inlet forced-feeding. In Fig. 6, the data measured with the compressor inlet forced-feeding at adiabatic conditions shows an extension to the right according to the adiabatic data already measured. The adiabatic hypothesis is the same as considered before: the turbine average temperature is equal to the compressor average temperature and the oil inlet temperature. The power consumed by the

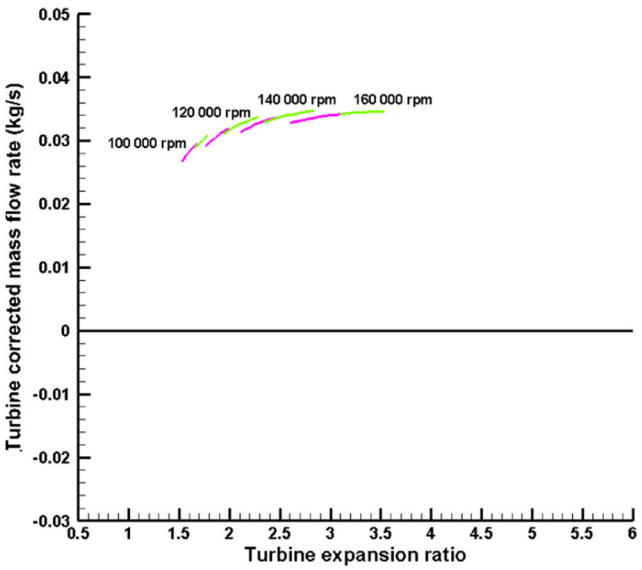

Fig. 6 Turbine corrected mass flow rate vs. turbine expansion ratio at adiabatic conditions (*purple*), and compressor inlet forced-feeding at adiabatic conditions (*light green*)

compressor is greater in this case and hereby the choke limit is shifted.

Compressor Exit Forced-Feeding On the surge limit side, the compressor performance is limited by the risk of entering a surge cycle. Surge is a self-excited cyclic phenomenon, affecting the compression system as a whole, characterized by large amplitude pressure rise and annulus averaged mass flow fluctuations [30]. Sometimes a reversed flow can take place. The surge phenomenon happens when the flow rate decreases in some components of the compressor and the whole system becomes unstable, hence generating surge.

To avoid this risk, air was blown to the compressor exit, hereby increasing the pressure on the backside of the blades and decreasing power consumed by the compressor. This way, it was possible to extend the turbine performance maps to the left (on the side of the surge limit).

With this technique, it is not possible to control the compressor inlet and exit temperature, so it was not possible to carry out this experiment in adiabatic conditions. However a turbine inlet temperature variation was done to extend as much as possible the measured data. Two turbine inlet temperatures were fixed: 300 °C and 100 °C.

The results for the 300 °C temperature are shown in Fig. 7: the data measured with the compressor exit forced-feeding is an extension of the data measured on the conventional test rig. The extension concerns the left side for high rotational speeds (160 000 rpm and 180 000 rpm corrected rotational speeds) as predicted. But for low rotational speeds (100 000 rpm corrected rotational speed and less), the curves are extended on both sides (right and left) and match with the data measured with the other techniques. So the compressor exit forced-feeding is more effective than predicted: it could extend the data map on the surge and choke limit sides.

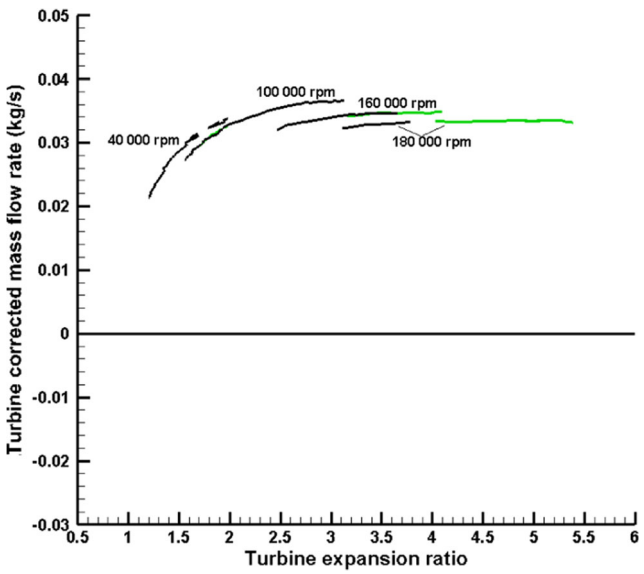

Fig. 7 Turbine corrected mass flow rate vs. turbine expansion ratio for turbine inlet temperature 300 °C (*green*), and compressor exit forced-feeding at turbine inlet temperature 300 °C (*black*)

Figure 8 shows the extension given by this technique to the left of the adiabatic data already measured, in the case of compressor exit forced-feeding and turbine inlet temperature of 100 °C. For some rotational speeds, it extends to the right side also and matches with the conventional test rig adiabatic data and the adiabatic data with the compressor inlet forced-feeding.

Compressor Replacement

All the techniques presented above allowed a considerable extension of the turbine mass flow rate performance map. In all these techniques, the turbocharger was not radically modified: the turbine and the compressor were intact. Only the flow inlet and exit conditions were changed. The results showed an extension of the initial turbine mass flow rate performance map but there is still a gap for lower mass flow rates at different rotational speeds.

Measurements using the mass flow meter

In this part, the compressor (shown in Fig. 9) was replaced by another one (shown in Fig. 10) with a different rotational sense. Air was blown to the new compressor exit. This way, the compressor worked as a turbine and helped the rotation of the turbine. So the turbine was able to turn at higher rotational speeds for the same mass flow rate and hereby extend the curves to higher expansion ratios. It was then possible to measure data at higher expansion ratios for low mass flow rates.

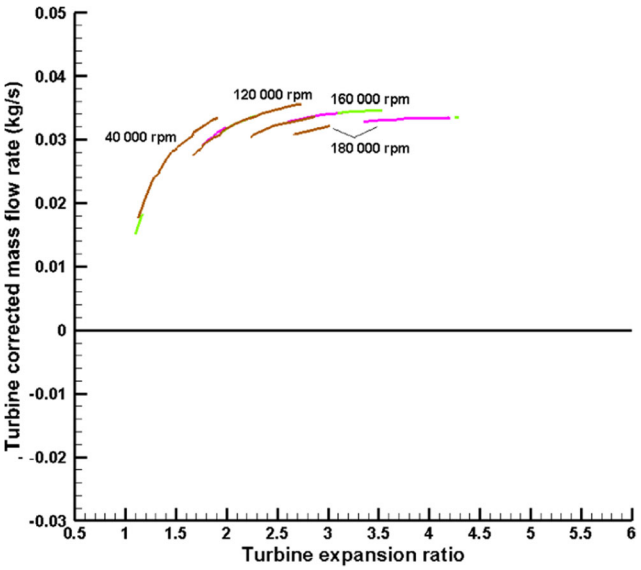

Fig. 8 Turbine corrected mass flow rate vs. turbine expansion ratio at compressor exit forced-feeding ($T_{in,turb} = 100$ °C) *brown*, traditional measurements at adiabatic conditions (*purple*) and compressor inlet forced-feeding at adiabatic conditions (*light green*)

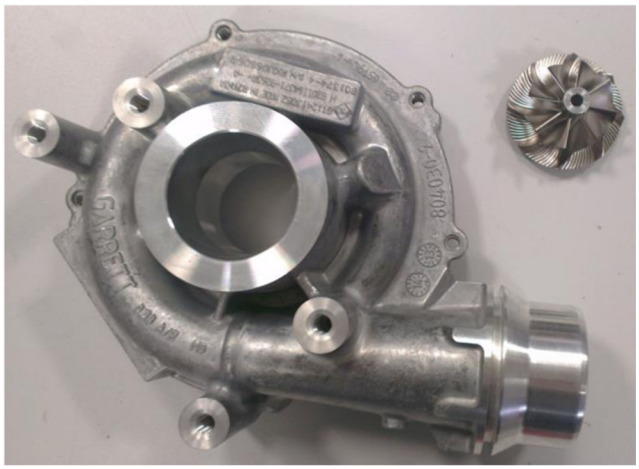

Fig. 9 Original compressor casing and rotor

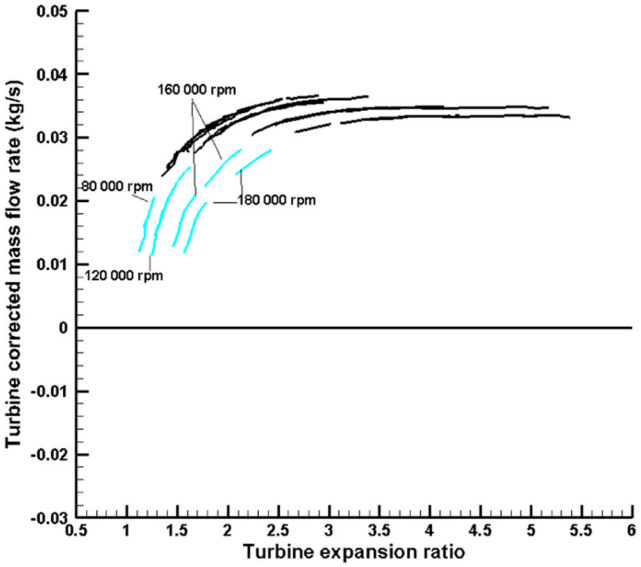

Fig. 11 Turbine corrected mass flow rate vs. turbine expansion ratio with the new compressor and turbine mass flow meter (*cyan*) and all the previously measured data (*black*)

Figure 11 shows the data measured with the new compressor and using the turbine mass flow meter mentioned in "Turbocharger presentation" section. The use of this mass flow meter was the main reason for the measure limitation for low mass flow rates. So another technique was used to extend the measurements for lower mass flow rates.

Measurements using the hot wire anemometer

Positive Mass Flow Rate Measurement As mentioned above, the compressor replacement allowed a measurement of lower mass flow rates for different rotational speeds and expansion ratios, but there was a limitation by the turbine mass flow meter so it was not possible to measure mass flow rates lower than 50 kg/h. Another technique was then used to measure lower turbine mass flow rates: a hot wire anemometer. This anemometer (shown in Fig. 12) allows to measure low mass flow rates as we can see in Fig. 13.

The hot wire anemometer is an instrument to measure gases velocity, especially fast velocity gases and velocity fluctuations. It works on the basis of convective heat transfer from a heated sensor to the surrounding fluid, the heat transfer being primarily related to the fluid velocity. By using very fine wire sensors placed in the fluid and electronics with servo-loop technique, it is possible to measure velocity fluctuations of fine scale of high frequencies [31].

Negative Mass Flow Rate Measurement To go further and extend the curves the most, an experiment was done to measure the mass flow rate at an expansion ratio of 1. With a rotating turbine and a pressure drop inside the turbine, the mass flow rate at an expansion ratio of one should be negative.

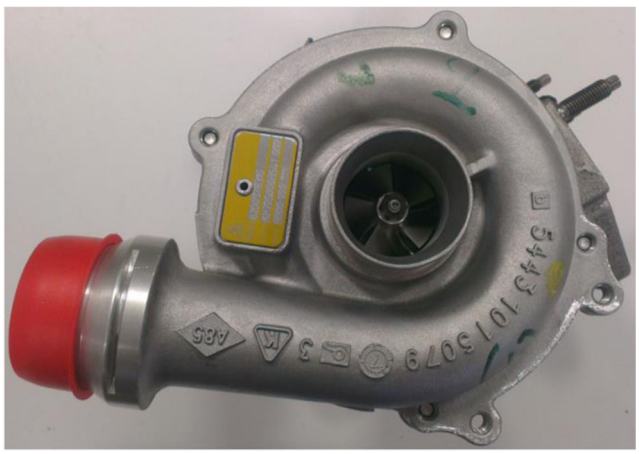

Fig. 10 New compressor casing and rotor (inside)

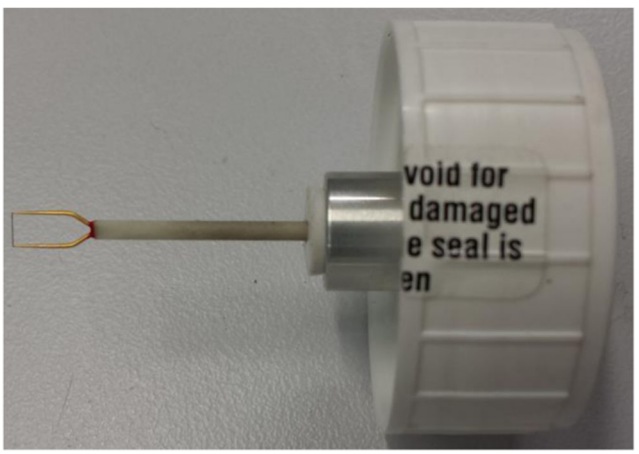

Fig. 12 Hot wire anemometer probe

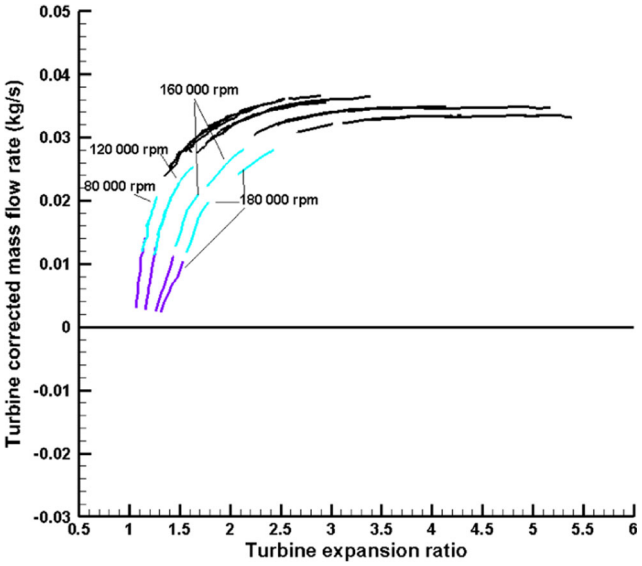

Fig. 13 Turbine corrected mass flow rate vs. turbine expansion ratio with the new compressor and the hot wire anemometer (*mauve*), the new compressor with the turbine mass flow meter (*cyan*) and all the previously measured data (*black*)

The assembly with the new compressor presented above was used, but the turbine is now driven by the compressor (Figs. 14 and 15). The turbine mass flow rate is measured using the hot wire anemometer described before. This one is mounted at the turbine exit (which in this case is the air inlet), to measure the flow before entering the turbine where it could be mixed with oil. Additionally a flow rectifier is implemented to avoid

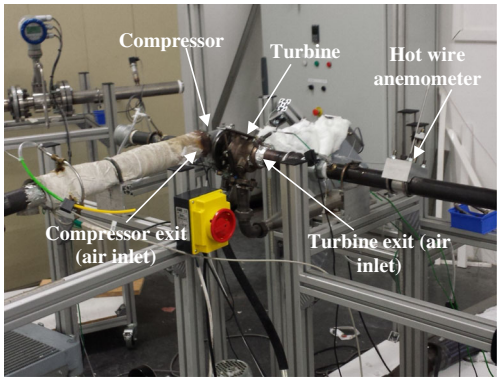

Fig. 15 Turbocharger test rig photo: negative flow measurements

turbulences. Air is then introduced into the turbine and evacuated: at the turbine inlet (in this case the air exit), there was an electric vane to create a pressure drop and measure higher expansion ratios. The data measured is presented in red in Fig. 16 where we can see negative flows for expansion ratios going from 1 to higher.

The flow measured is negative since it goes through the turbine in the opposite direction, and the temperature used for the corrected values is the turbine exit temperature (the air inlet temperature). As shown in (equations (1) and (2)), the turbine inlet temperature and pressure are used in the calculation of the corrected mass flow rate and rotational speed, but in this case the temperature and the pressure used will be the turbine exit temperature and pressure since they are the air inlet temperature and

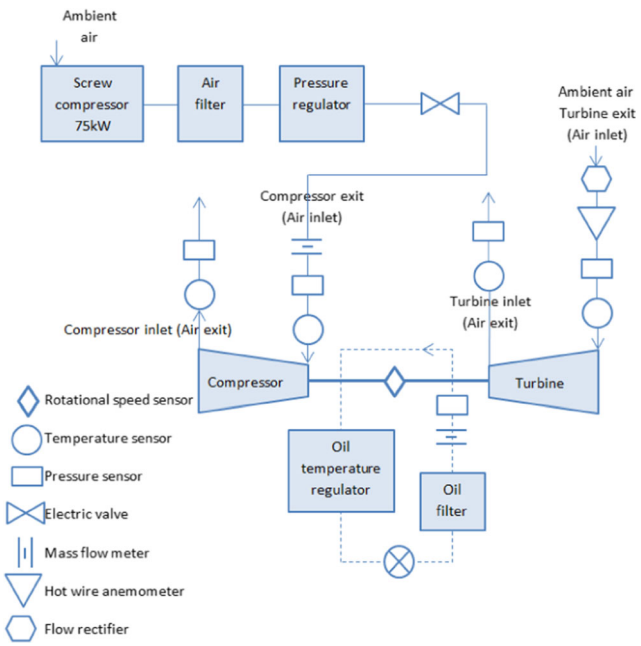

Fig. 14 Turbocharger test rig: new compressor installed, negative turbine mass flow rate measurements

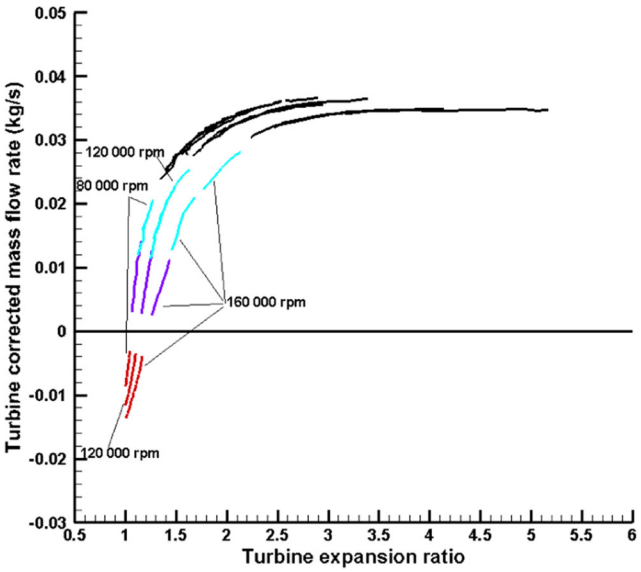

Fig. 16 Turbine corrected mass flow rate vs. turbine expansion ratio with the new compressor and the hot wire anemometer at negative mass flow rate (*red*), with the new compressor and the hot wire anemometer at positive mass flow rate (*mauve*), the new compressor with the turbine mass flow meter (*cyan*) and all the previously measured data (*black*)

pressure. The fluid inlet temperature and pressure are the ones that should be used in the corrected values equations. In this case the equations are different as we can see in (equations (8) and (9)):

$$D_{m-corr} = D_m \times \frac{\sqrt{\frac{T^*_{out,turb}}{T_{ref}}}}{\frac{P^*_{out,turb}}{P_{ref}}} \tag{8}$$

$$N_{corr} = N \times \sqrt{\frac{T_{ref}}{T^*_{out,turb}}} \tag{9}$$

Conclusion

With this last set of data added to the performance map, this one becomes almost complete. To achieve that, the techniques used were the turbine inlet temperature variation, the compressor inlet and exit forced-feeding, and the compressor exchange. With the turbine inlet temperature variation, the air density allowed to measure different zones on the performance map. With the compressor forced-feeding, it was possible to increase the power consumed by the compressor (compressor inlet forced-feeding) and shift the surge limit (compressor exit forced-feeding). The compressor change enabled to measure low positive and negative mass flows and reach low expansion ratios until 1. Entire turbine mass flow rate performance map is presented in Fig. 17.

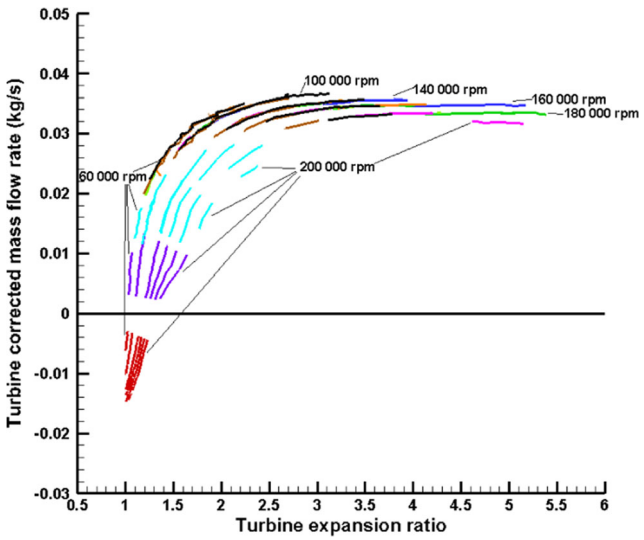

Fig. 17 Entire turbine mass flow rate performance map: turbine corrected mass flow rate vs. turbine expansion ratio with the different measurement techniques (see color index for each technique in Table 1)

Turbine Efficiency Measurements

The supplier usually gives the turbine efficiency as the result of the product of the turbine isentropic efficiency (total-to-static) and the turbocharger mechanical efficiency). It is the ratio of the power consumed by the compressor to the power produced by the turbine in isentropic conditions.

$$\eta_{turb} = \eta_{t-s} \times \eta_{meca} \tag{10}$$

$$\eta_{turb} = \frac{P_{comp}}{P_{turb,isentr}} \tag{11}$$

The choice of this efficiency is because of the non-adiabatic conditions on the traditional turbocharger test rig. At non adiabatic conditions, it is not possible to distinguish the turbine isentropic efficiency and the turbocharger mechanical efficiency. In this study, using the adiabatic conditions results, it is possible to calculate separately the turbine isentropic efficiency and the turbocharger mechanical efficiency.

Turbine Isentropic (Total-to-Static) Efficiency

The turbine isentropic (total-to-static) efficiency is the ratio between the power produced by the turbine during the fluid expansion, and the power produced by the turbine at an isentropic expansion.

$$\eta_{t-s} = \frac{P_{turb}}{P_{turb,isentr}} = \frac{h^*_{in-turb} - h^*_{out-turb}}{h^*_{in-turb} - h_{out-isentr}} \tag{12}$$

For adiabatic conditions and considering an ideal gas, the isentropic efficiency equation becomes:

$$\eta_{t-s} = \frac{T^*_{in-turb} - T^*_{out-turb}}{T^*_{in-turb} - T_{out-isentr}} \tag{13}$$

The only conditions in our experiments that could give suitable data are the tests performed on the "traditional" turbocharger test rig at adiabatic conditions (see paragraph 1.1.2), and the compressor inlet forced-feeding at adiabatic conditions (see paragraph 1.1.3.1). The rest of the data are not relevant for these calculations.

The results of this turbine isentropic efficiency appear in Fig. 18. It shows the curves increasing and then decreasing with the corrected rotational speed. Each corrected rotational speed has a maximum of isentropic (total-to-static) efficiency which corresponds to its optimal operating point. If we take all the efficiency curves, it is visible that the efficiency grows with the rotational speed until 140 000 rpm (corrected rotational speed) and then decreases. A possible explanation is that the aerodynamic losses reach their minimum for optimal operating points.

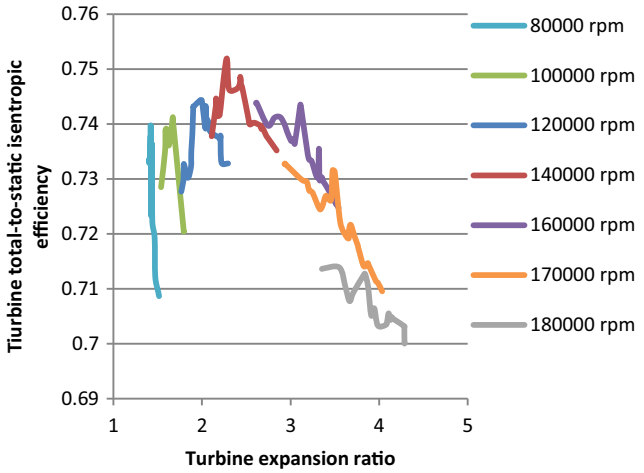

Fig. 18 Turbine isentropic (total-to-static) efficiency vs. turbine expansion ratio (adiabatic data)

Turbocharger Mechanical Efficiency

The mechanical efficiency of a turbocharger is the ratio between the power consumed by the compressor and the power produced by the turbine. So the mechanical power loss is the friction power loss on the shaft.

$$\eta_{meca} = \frac{P_{comp}}{P_{turb}} = \frac{P_{comp}}{P_{comp} + P_{friction}} \tag{14}$$

The studied turbocharger is equipped with oil bearings. There are journal bearings for the shaft rotation and an axial thrust bearing to carry the axial load due to the force imbalance between the turbine wheel and the compressor wheel [4]. With this type of turbochargers, the mechanical efficiency is assumed to be constant and at a high value at high rotational speeds. For lower rotational speeds, the power provided to the compressed air is reduced and the mechanical efficiency is no longer constant nor high [5].

Adiabatic conditions enable to calculate the power produced and consumed via the total enthalpy difference. Using the first principle of thermodynamics and considering the air as an ideal gas, we can obtain the power produced by the turbine and the power consumed by the compressor:

$$P_{comp} = Dm_{comp}\left(h^*_{out,comp} - h^*_{in,comp}\right) \tag{15}$$

$$P_{comp} = Dm_{comp}.c_{p-air}\left(T^*_{out,comp} - T^*_{in,comp}\right) \tag{16}$$

$$P_{turb} = Dm_{turb}\left(h^*_{in,turb} - h^*_{out,turb}\right) \tag{17}$$

$$P_{turb} = Dm_{turb}.c_{p-air}\left(T^*_{in,turb} - T^*_{out,turb}\right) \tag{18}$$

The turbocharger mechanical efficiency expression becomes:

$$\eta_{meca} = \frac{Dm_{comp}.c_{p-air}\left(T^*_{out,comp} - T^*_{in,comp}\right)}{Dm_{turb}.c_{p-air}\left(T^*_{in,turb} - T^*_{out,turb}\right)} \tag{19}$$

Using (equation (19)), it is possible to calculate the turbocharger mechanical efficiency. The results are shown in Fig. 19. As expected, the turbocharger mechanical efficiency grows with the rotational speed until it gets its maximum value and becomes constant: It is also clear that for the corrected rotational speeds of 100 000 rpm, 120 000 rpm and 130 000 rpm the curve of the mechanical efficiency has a maximum that corresponds to an optimal functioning point (as it was the case for the turbine isentropic efficiency).

Turbine Manufacturer Efficiency

The turbine efficiency maps given by the supplier represent the product of the two efficiencies presented above: the turbine isentropic efficiency and the turbocharger mechanical efficiency (see equation (10)). However the data given by the supplier is usually calculated using data measured with a turbine inlet temperature of 600 °C or more. So there is an important impact of the heat transfers on the efficiency calculation: the mechanical efficiency and the isentropic efficiency equations are based on the hypothesis of an adiabatic process which is not the case at such high temperatures.

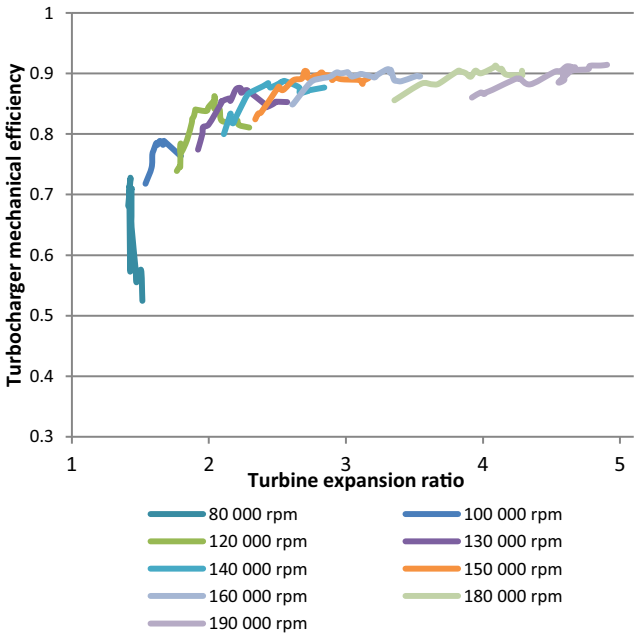

Fig. 19 Turbocharger mechanical efficiency vs. turbine expansion ratio (adiabatic data)

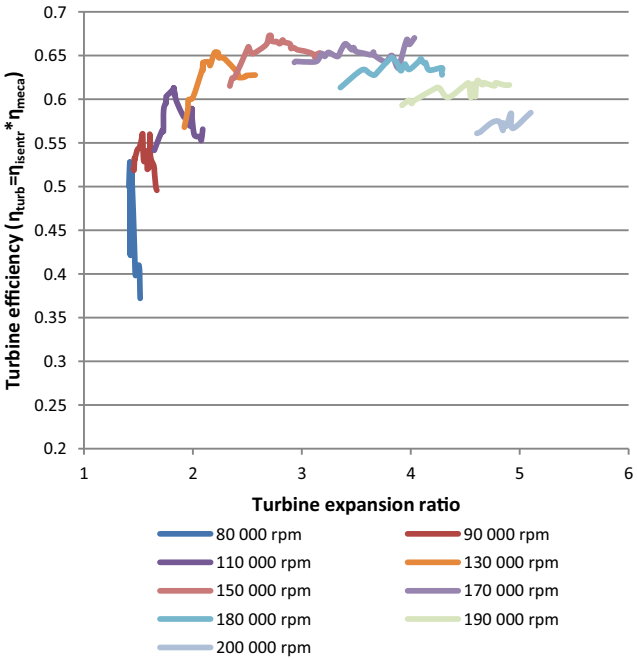

Fig. 20 Turbine efficiency ($\eta_{turb} = \eta_{isentr} * \eta_{meca}$) vs. turbine expansion ratio (adiabatic data)

The turbine efficiency given by the supplier can be calculated using (equation (11)). Considering an adiabatic process inside the compressor and an ideal gas going through the turbine and the compressor, (equation (11)) becomes:

$$\eta_{turb} = \frac{Dm_{comp}.c_{p-air}\left(T^*_{out,comp} - T^*_{in,comp}\right)}{Dm_{turb}.c_{p-air}\left(T^*_{in-turb} - T_{out-isentr}\right)} \quad (20)$$

This expression of the turbine efficiency can be used with the condition of an adiabatic process in both the compressor and the turbine. Otherwise, the heat transfers

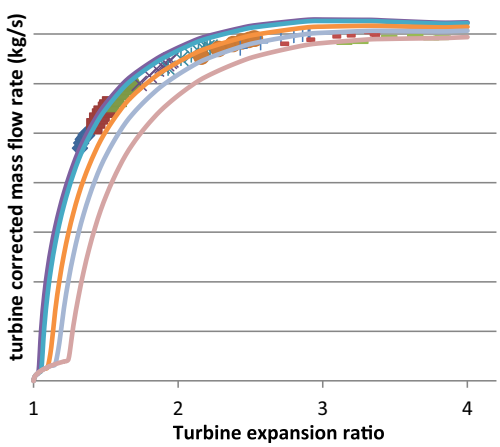

Fig. 21 GT Power software extrapolation of turbine corrected mass flow rate vs. turbine expansion ratio

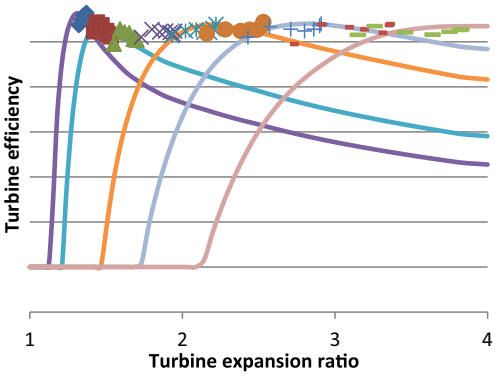

Fig. 22 GT Power software extrapolation of turbine eficiency vs. turbine expansion ratio

effect occurs. Considering the compressor side: if there is a heat transfer from the turbine to the compressor, then the first principle applied to the compressor will give us the equation:

$$P_{comp} = Dm_{comp}.c_{p-air}\left(T^*_{out,comp} - T^*_{in,comp}\right) - Q \quad (21)$$

Where Q is the amount of the heat gained by the air in the compressor during the compression. This quantity Q can be neglected if the process is adiabatic which is not the case with the manufacturer's data. Otherwise, the data presented in this part are adiabatic. The calculation can then be done either by using an equation for the turbine efficiency (equation (20)) or by using the two efficiencies calculated separately (equations (13) and (19)) but the result is not comparable to the data given by the manufacturer.

Figure 20 shows the results of the calculation of the turbine efficiency defined by the manufacturer. The shape and the values of the curves were predictable

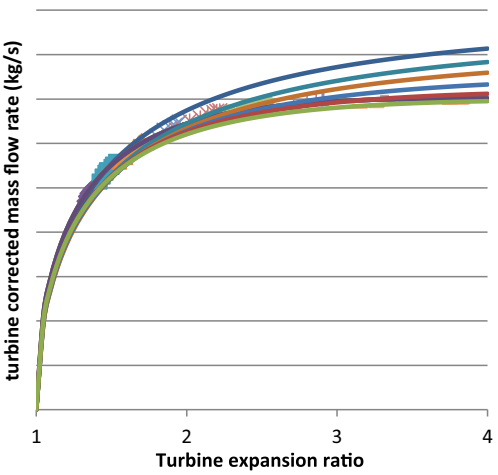

Fig. 23 AMESim software extrapolation of turbine corrected mass flow rate vs. turbine expansion ratio

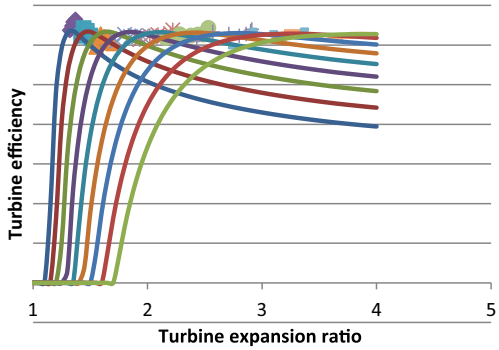

Fig. 24 AMESim software extrapolation of turbine efficiency vs. turbine expansion ratio

from the previous curves of the isentropic and mechanical efficiency. The turbine efficiency grows with the rotational speed until it gets to an optimal point around 140 000 rpm – 150 000 rpm (corrected rotational speed). This is explained by the fact that both the isentropic and the mechanical efficiencies increase. After this optimal region, the isentropic efficiency decreases (see Fig. 18) but the mechanical efficiency stays constant (see Fig. 19) so the turbine efficiency lightly decreases. For each rotational speed, as mentioned before, there is a maximum (optimal functioning point). It was the expected to have these optimal points for each rotational speed on the turbine efficiency (η_{turb}).

The measurement of the turbine isentropic efficiency and the turbocharger mechanical efficiency separately is important because it allows the study of each term separately. The main advantage of these results is the possibility to extrapolate the data map of each efficiency separately which is better than extrapolating the turbine efficiency directly: there is no physically based method in this case.

Simulation Models

In this section, we present the extrapolation of the turbine performance map given by the manufacturer using two commercial software: AMESim and GT power. Figure 21 shows the turbine corrected mass flow rate given by GT power; the shape of the curves is close to the ones measured experimentally but there is a difference in the data values. As for AMESim, Fig. 22 shows a different shape of turbine corrected mass flow rate curves. Figure 23 shows the turbine efficiency extrapolation using GT power while Fig. 24 shows the same efficiency extrapolation using AMESim. The shape of the curves is almost the same in both cases but it is not comparable to the data measured and calculated previously due to the difference in the measuring conditions between our adiabatic data and the manufacturer's as mentioned above. This experimental study is useful then to get a complete turbine performance map that will lead to a more accurate and precise extrapolation model.

Uncertainty Analysis

The parameters measured to determine the turbine and the compressor performance maps are: the turbine inlet mass flow rate, the turbine inlet and exit static temperature and pressure, the compressor inlet mass flow rate, the compressor inlet and exit static temperature and pressure, the atmospheric pressure and the turbocharger rotational speed.

Using a standard deviation of rectangular distribution, it is possible to calculate the uncertainty δ for the measured data shown in Table 2. Using these uncertainties, it is possible to calculate the uncertainty of the calculated data such as the efficiencies. The equations used and the uncertainty calculations are presented by Mohtar et al. [32].

Table 2 Manufacturer specification for each sensor

Sensor	Calibrated range	Accuracy, Δ	Uncertainty, δ
Temperature [T]: K-type Thermocouple	0–1000 °C	±1 °C	(1/√3)
Pressure [P]: Piezo resistive relative pressure sensor	0–100 mbar	±1.5 mbar	(1.5/√3)
	0–350 mbar	±5.25 mbar	(5.25/√3)
	0–1 bar	±15 mbar	(15/√3)
	0–2 bar	±30 mbar	(30/√3)
	0–5 bar	±75 mbar	(75/√3)
Pressure [P]: Atmospheric pressure sensor	0.8–1.1 bar	±3 mbar	(3/√3)
Rotational speed [N]: Inductive sensor (Picoturn)	0–300 000 rpm	±200 rpm	(200/√3)
Air mass flow rate [D_m] turbine: Vortex (Optiswirl 4070C)	$10^4 < Re < 2*10^4$	±2.5 %. D_m	([2.5 %.ṁ]/√3)
	$Re \geq 2*10^4$	±1.5 %. D_m	([1.5 %.ṁ]/√3)
Air mass flow rate [D_m] compressor: Vortex (Optiswirl 4200)	$10^4 < Re < 2*10^4$	±2.5 %. D_m	([2.5 %.ṁ]/√3)
	$Re \geq 2*10^4$	±1.5 %. D_m	([1.5 %.ṁ]/√3)

For the turbine isentropic efficiency, the uncertainties are around 5 % for high rotational speeds and expansion ratios (around 4 or 5) and can get up to 25 % for lower rotational speeds and expansion ratios (around 2). As for the mechanical efficiency, its uncertainty is around 8 % for high rotational speeds and expansion ratios (from 3 to 5) and can get up to 15 or 20 % for lower rotational speeds and expansion ratios (around 1.5 or 2). And for the turbine efficiency, its uncertainty is around 9 % for high rotational speeds and expansion ratios (around 4 or 5) and can get up to 30 % for lower rotational speeds and expansion ratios (around 2).

Conclusions and Perspectives

The work presented in this study shows that it is possible to extend a turbocharger radial turbine performance maps. For the mass flow rate performance map, it was possible to extend the data to almost the complete area with a turbine expansion ratio between 1 and 6 and corrected rotational speeds between 40 000 rpm and 200 000 rpm (see Fig. 17). For some of these rotational speeds, the curves are almost complete which is an important point considering the narrow area given by the manufacturer's data maps. The different techniques used in this study were: the turbine inlet temperature variation, the compressor inlet and exit forced-feeding and the compressor replacement. With this last technique, it was possible to measure very low mass flow rates and even negative mass flow rates with expansion ratio going until 1. This data will be used to improve the automotive models and create an extrapolation model of the turbine corrected mass flow rate performance map. The information will be useful in terms of values and curves shape.

The other point studied here is the turbine efficiency: the main advantage of this study is the measurement of the turbine isentropic efficiency and the turbocharger mechanical efficiency separately. This was possible with the data measured previously for the turbine mass flow rate but only in adiabatic conditions. As mentioned before, the calculation of the two efficiencies will allow the extrapolation of each one separately instead of extrapolating the turbine efficiency (η_{turb}). It is possible even more to develop a model for each one and hereby get a complete model of the turbine performance: mass flow rate and efficiency.

Acknowledgments The authors wish to acknowledge Renault, Siemens, and Ecole Centrale de Nantes, members of the industrial chair financing this project. The industrial chair entitles "system modeling for the control and calibration of internal combustion engines".

References

1. SAE J1826, issued 1989–04. Reaffirmed 1995–03.: Turbocharger stand test code. (1995)
2. Venson GG, Barros JEM (2008) Turbocharger performance maps building using a hot gas test stand. Proceedings of ASME Turbo Expo 2008: power for land, sea and air GT2008 june 9–13, 2008, GT2008-509, Berlin, Germany
3. Otobe T (2010) Method of performance measurement for low turbocharger speeds. 15 th supercharging conference, Dresden, Germany
4. Deligant M et al (2012) Experimental identification of turbocharger mechanical friction losses. Energy. doi:10.1016/j.energy.2011-12-049
5. Deligant M, Podevin P, Lamquin T, Vidal F et al (2010) Experimental study of turbocharger's performances at low speeds. ASME 2010 internal combustion engine division fall technical conference: 1–8. doi:10.1115/ICEF2010-35071
6. Lamquin T, Gjika K (2009) Power losses identification on turbocharger hydrodynamic bearing. Proceedings of ASME Turbo Expo, Power for Land, Sea and Air, Orlando, FL USA. doi:10.1115/GT2009-59599
7. Podevin P, Descombes G, Clenci A, Zaharia C (2004) Researches regarding mechanical efficiency evaluation at turbochargers. Proceeding of the International Automotive Congress, Brasov, Romania
8. Podevin P, Toussaint M, Richard G, Farinole G (2002) Performances of turbocharger at low speed. Proceeding of the SYMKOMO2 congress, Lodz, Pologne
9. Scharf J, Schorn N, Smiljanovski V, Uhlmann T, Aymanns R (2010) Methods for extended turbocharger mapping and turbocharger assessment. 15th superchanrging conference, Dresden, Germany
10. Dale AP (1990) Radial, vaneless, turbocharger turbine performance. Ph.D. thesis, University of London, UK
11. Winterbone DE, Nikpour B, Alexander GI (1990) Measurement of the performance of a radial inflow turbine in conditional steady and unsteady flow. IMeche Paper No. C405(015) : 153–162
12. Nikpour B (1990) Measurement of the performance of a radial inflow turbine. Ph.D. thesis. University of Manchester, Institute of Science and Technology
13. Arcoumanis C, Hakeem I, Khezzar L, Martinez-Botas RF et al (1995) Performance of a mixed flow turbocharger turbine under pulsating flow conditions. ASME International gas turbine and aeroengine congress and exposition (95-GT-210)
14. Szymko S (2006) The development of an eddy current dynamometer for evaluation of steady and pulsating turbocharger turbine performance. Ph.D. thesis, Imperial College London
15. Payri F, Serrano JP, Fajardo P, Reyes-Belmonte MA et al (2012) A physically based methodology to extrapolate performance maps of radial turbines. Energy Convers Manag 55:149–163. doi:10.1016/j.enconman.2011.11.003
16. Galindo J, Serrano JR, Guardiola C, Cervello C (2006) Surge limit definition in a specific test bench for the characterization of automotive turbochargers. Exp Therm Fluid Sci 30:449–462. doi:10.1016/j.expthermflusci.2005.06.002
17. CIMAC (The International Council on Combustion Engines) (2007) Turbocharging efficiencies - definitions and guidelines for measurement and calculation. CIMAC working group 'Turbocharger Efficiency'. Number 27/2007
18. Watson N, Janota MS (1982) Turbocharging the internal combustion engine. Wiley (ISBN: 0471870722, 9780471870722)
19. Payri F, Desantes JM, Boada F (1986) Prediction method for the operating conditions of a turbocharged diesel engine. Proc. of the Motor Sympo'86 (2): 8–16

20. Winterbone DE. The theory of wave action approaches applied to reciprocating engines. Internal combustion engineering: science & technology. pp 445–500, Springer Netherlands. doi: 10.1007/978-94-009-0749-2_121990, print ISBN: 978-94-010-6822-2, online ISBN: 978-94-009-0749-2)
21. Hibernik A, Dobovisek Z, Cernej A (1994) Application of rotor characteristics for one-dimensional turbine modelling. Proc Inst Mech Eng C 484(034):239–249
22. Payri F, Benajes J, Reyes M (1996) Modelling of supercharger turbines in internal-combustion engines. Int J Mech Sci 38(8–9): 853–869. doi:10.1016/0020-7403(95)00105-0)
23. Payri F, Benajes J, Jullein J, Duan Q (1991) Non-steady flow behaviour of supercharger turbine. Proc. of the third EAEC international conference: 347–51., Strasbourg
24. Chen H, Hakeem I, Martinez-Botas R (1996) Modelling of a turbocharger turbine under pulsating inlet conditions. Proc Inst Mech Eng 210:397–407
25. Macek J, Vavra J (2002) 1-D model of radial turbocharger turbine calibrated by experiments. SAE Technical Paper 2002-01-0377. doi:10.4271/2002-01-0377
26. Nasser SH, Playfoot BB (1999) A turbocharger selection computer model. SAE Technical Paper 1999-01-0559. doi:10.4271/1999-01-0559
27. Frelin M (1991) Prévision des caractéristiques d'une turbine radiale à partir des données géométriques. Ph.D. thesis, Université Paris 6
28. Cormerais M, Chesse P, Hetet JF, Yammine A (2008) Experimental characterisation and modelling of turbocharger heat transfers under steady and transient conditions. The 12th International Symposium on Transport Phenomena and Dynamics of Rotating Machinery, Paper ISROMAC12-2008-20006
29. Cormerais M, Hetet JF, Chesse P, Maiboom A (2006) Heat transfers characterisations in a variable geometry turbocharger: experimental and correlations. ASME conference paper ICES2006-1324
30. Pampreen RC (1993) Compressor surge and stall. Concepts ETI, Incorporated. ISBN: 0933283059, 9780933283053
31. (2004) Mini CAT Anemometer Package, how to get started - a quick guide. Dantec Dynamics, Skovlunde, Denmark
32. Mohtar H, Chesse P, Chalet D (2012) Describing uncertainties encountered during laboratory turbocharger compressor tests. Soc Exp Mech. doi:10.1111/j.1747-1567.2011.00734.x